Strong current sheet at a magnetosheath jet: Kinetic structure and electron acceleration

E. Eriksson, A. Vaivads, D. B. Graham, Yu. V. Khotyaintsev, E. Yordanova, H. Hietala, M. André, L. A. Avanov, J. C. Dorelli, D. J. Gershman, et al.

AGU PUBLICATIONS

JGR

Journal of Geophysical Research: Space Physics

RESEARCH ARTICLE
10.1002/2016JA023146

Strong current sheet at a magnetosheath jet: Kinetic structure and electron acceleration

E. Eriksson[1,2], A. Vaivads[1], D. B. Graham[1], Yu. V. Khotyaintsev[1], E. Yordanova[1], H. Hietala[3], M. André[1], L. A. Avanov[4], J. C. Dorelli[4], D. J. Gershman[4,5], B. L. Giles[4], B. Lavraud[6], W. R. Paterson[4], C. J. Pollock[4], Y. Saito[7], W. Magnes[8], C. Russell[3], R. Torbert[9], R. Ergun[10], P-A. Lindqvist[11], and J. Burch[12]

[1]Swedish Institute of Space Physics, Uppsala, Sweden, [2]Department of Physics and Astronomy, Uppsala University, Uppsala, Sweden, [3]Department of Earth and Space Sciences, University of California, Los Angeles, California, USA, [4]NASA Goddard Space Flight Center, Greenbelt, Maryland, USA, [5]Department of Astronomy, University of Maryland, College Park, Maryland, USA, [6]IRAP, CNRS, Toulouse, France, [7]JAXA, Chofu, Japan, [8]Space Research Institute, Austrian Academy of Sciences, Graz, Austria, [9]Space Science Center, University of New Hampshire, Durham, New Hampshire, USA, [10]Laboratory of Atmospheric and Space Physics, University of Colorado Boulder, Boulder, Colorado, USA, [11]KTH Royal Institute of Technology, Stockholm, Sweden, [12]Southwest Research Institute, San Antonio, Texas, USA

Abstract Localized kinetic-scale regions of strong current are believed to play an important role in plasma thermalization and particle acceleration in turbulent plasmas. We present a detailed study of a strong localized current, 4900 nA m^{-2}, located at a fast plasma jet observed in the magnetosheath downstream of a quasi-parallel shock. The thickness of the current region is ~3 ion inertial lengths and forms at a boundary separating magnetosheath-like and solar wind-like plasmas. On ion scales the current region has the shape of a sheet with a significant average normal magnetic field component but shows strong variations on smaller scales. The dynamic pressure within the magnetosheath jet is over 3 times the solar wind dynamic pressure. We suggest that the current sheet is forming due to high velocity shears associated with the jet. Inside the current sheet we observe local electron acceleration, producing electron beams, along the magnetic field. However, there is no clear sign of ongoing reconnection. At higher energies, above the beam energy, we observe a loss cone consistent with part of the hot magnetosheath-like electrons escaping into the colder solar wind-like plasma. This suggests that the acceleration process within the current sheet is similar to the one that occurs at shocks, where electron beams and loss cones are also observed. Therefore, electron beams observed in the magnetosheath do not have to originate from the bow shock but can also be generated locally inside the magnetosheath.

Key Points:
- MMS observations of strong ion scale current sheet forming at a magnetosheath jet
- Local field-aligned electron acceleration at current sheet
- The acceleration mechanism is similar to the one observed at shocks

Correspondence to:
E. Eriksson,
elin.eriksson@irfu.se

Citation:
Eriksson, E., et al. (2016), Strong current sheet at a magnetosheath jet: Kinetic structure and electron acceleration, *J. Geophys. Res. Space Physics*, *121*, 9608–9618, doi:10.1002/2016JA023146.

Received 7 JUL 2016
Accepted 20 SEP 2016
Accepted article online 28 SEP 2016
Published online 12 OCT 2016

1. Introduction

The magnetosheath downstream of a quasi-parallel shock is one of the most turbulent plasma environments in the near-Earth space [*Retino et al.*, 2007], where large variations are observed in the magnetic field, plasma density, and velocity. In this turbulent environment, plasma is efficiently thermalized [*Retino et al.*, 2007; *Chasapis et al.*, 2015] and particles accelerated to suprathermal energies have been observed there [*Retino et al.*, 2007]. However, the plasma thermalization and particle acceleration processes are still not fully understood. Strong localized kinetic-scale currents are believed to play an important role in these processes [*Priest and Forbes*, 2000; *Birn and Priest*, 2007; *Karimabadi et al.*, 2014]. Such localized current sheets are ubiquitous in the magnetosheath downstream of quasi-parallel shocks [*Greco et al.*, 2008; *Servidio et al.*, 2009; *Wan et al.*, 2015; *Vörös et al.*, 2016]. Magnetic reconnection processes can start in those current sheets leading to plasma heating and particle acceleration [*Retino et al.*, 2007; *Karimabadi et al.*, 2014; *Chasapis et al.*, 2015; *Yordanova et al.*, 2016]. Simulations suggest that a possible generator of those current sheets can be localized dynamic pressure enhancements often called (high-speed) jets [*Karimabadi et al.*, 2014; *Hao et al.*, 2016; *Omidi et al.*, 2016]. These jets have also been observed in spacecraft data [*Plaschke et al.*, 2013; *Archer and Horbury*, 2013], but their relation to current sheet formation is not fully understood. Numerical simulations and theory suggest that velocity shears can contribute to the formation of current sheets [*Mikhailovskii*, 1974; *Servidio et al.*, 2015]. So far, due to instrumental limitations of earlier missions, a detailed description of all these processes at kinetic scales has been lacking. To understand current sheet formation and processes leading

to plasma heating and particle acceleration within thin current sheets, it is important to have high temporal resolution particle data.

The new Magnetospheric Multiscale (MMS) mission [*Burch et al.*, 2016] provides greatly improved particle measurements with a small spacecraft separation, making it possible for the first time to perform detailed studies of the kinetic processes occurring inside thin current sheets. MMS measures the electron and ion distribution functions at sufficiently high cadence (30 and 150 ms, respectively) to resolve kinetic scales. In addition, the MMS apogee during the first year has been far enough from Earth that during periods of high solar wind pressure MMS crossed the bow shock for short time intervals. Thus, the magnetosheath at different distances from the shock could be sampled. MMS has already collected data from many events within the magnetosheath regions downstream of a quasi-parallel shock, and it is important to carry out both detailed event studies as well as statistical studies to understand the major physical processes leading to plasma heating and particle acceleration there.

In this paper we present a detailed study of a strong, kinetic-scale magnetosheath current sheet, located in a magnetosheath jet region, and its related electron acceleration. The paper is organized as follows: section 2.1 gives an overview of the region where the strong current sheet is observed, section 2.2 presents the current sheet, in section 3 we discuss the current sheet formation and the electron beam observed in the current sheet, and in section 4 we give our conclusions.

2. Event Overview

2.1. Large-Scale Context

We present MMS observations of the magnetosheath, downstream of a quasi-parallel shock, on 30 November 2015 when MMS was at [8, −3, −0.5]*Re* in Geocentric Solar Ecliptic (GSE) coordinates. During this period the spacecraft separation was 20 km, which is comparable to the ion inertial length ($\lambda_i \sim 23$ km) and thus allows detailed kinetic studies of the current region. We use magnetic field **B** data from the fluxgate magnetometer (FGM) [*Russell et al.*, 2016], electric field **E** data from the FIELDS electric field double probes instrument [*Lindqvist et al.*, 2016; *Ergun et al.*, 2016], and particle data from the fast plasma investigation (FPI) instrument [*Pollock et al.*, 2016]. We also use OMNI [*King and Papitashvili*, 2005] data to determine the undisturbed solar wind parameters during the event. The fast solar wind ($V_{SW} = 465$ km s^{-1}) has a very high density ($n_{SW} = 19$ cm^{-3}); and therefore, the solar wind dynamic pressure P_{dyn}^{SW} (∼7 nPa) is much larger than normally observed values leading to a highly compressed magnetosheath. The predicted IMF orientation during the selected event is [−7.0, 3.0, −3.0] nT in GSE, corresponding to a shock angle of 27° [*Farris and Russell*, 1994; *Shue et al.*, 1998] with respect to the shock normal at the spacecraft location. Thus, MMS was located in the magnetosheath downstream of a quasi-parallel shock.

Figure 1 shows a 1.5 min overview from MMS4 surrounding the selected current region (highlighted in orange). The violet areas indicates regions of magnetosheath jets according to the *Plaschke et al.* [2013] identification criterion which is also explained later in the text. The data from the four spacecraft are very similar over large scales, due to the small spacecraft separation, thus we primarily show data from MMS4. During the whole interval MMS is in the turbulent magnetosheath downstream of the bow shock. The magnetic field, Figure 1a, shows variations on different scales in all components including the magnitude of the field. There is a strong magnetic field increase, up to about 100 nT, right when the current peaks. Figure 1b shows the current calculated using the four-spacecraft curlometer method [*Dunlop et al.*, 1988]. During the whole time interval there are many regions with strong current; the strongest current region ($J > 4000$ nA m^{-2}) is analyzed in this paper.

Figures 1c–1e show the ion and electron velocities, and densities, respectively. The magnitude of the ion velocity is ∼200 km s^{-1} for the whole event, except around 00:24:20–00:24:30 UT where it reaches almost 300 km s^{-1}. The strong current region is embedded in this high flow region. The predominant direction of the ion velocity throughout the interval is $-X$, but there are large variations in the velocity direction, clearly showing the turbulent nature of the flow. Over large scales, the electron velocity (Figure 1d) is similar to the ion velocity but there are narrow regions of increased electron speed that in most cases coincide with regions of strong currents. The current region selected for this study is associated with a peak electron speed of ∼500 km s^{-1}. Throughout the interval, the density (Figure 1e) is well above the solar wind density, consistent with the spacecraft being in the magnetosheath. In localized regions density peaks can reach well above 200 cm^{-3}. Near one such density peak region is the location of the selected current region.

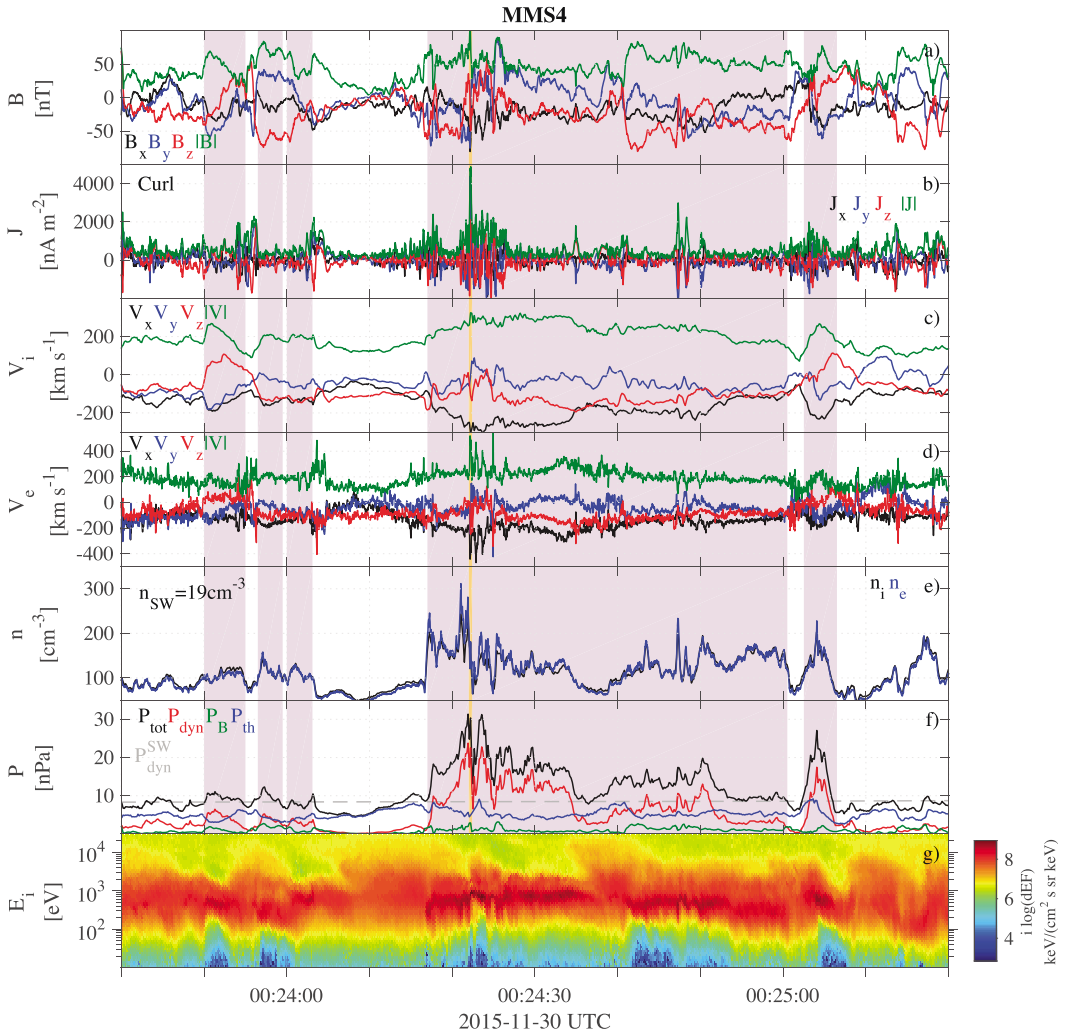

Figure 1. Overview of the event, where the orange shaded area indicates the studied current region. The violet areas indicate regions of magnetosheath jets using *Plaschke et al.* [2013] identification criterion (see text for details). Unless otherwise stated, all coordinates are in GSE. (a) Magnetic field; (b) current; (c) ion velocity; (d) electron velocity; (e) plasma density, ions (black), and electrons (blue); (f) total (black), dynamic (red), magnetic (green), and thermal (blue) pressure where the grey dotted line gives the solar wind dynamic pressure; and (g) omnidirectional ion flux.

Figure 1f shows the different plasma pressures. The solar wind dynamic pressure in the *x* direction calculated from the OMNI data is marked with a dotted grey line. In a stationary situation the total pressure in the magnetosheath would be balanced by the solar wind dynamic pressure, $P_{dyn}^{SW} = \rho_{SW} V_{SW,x}^2$. However, we see that the total pressure P_{tot} observed by the spacecraft is varying, and in several regions it is several times larger than P_{dyn}^{SW}. When looking at the different components of the P_{tot}, we can see that in the regions of high pressure the dynamic pressure, $P_{dyn} = \rho_i V_{i,x}^2$, is dominant. Furthermore, we observe both density and plasma speed increases in these regions that contribute to the increase in P_{dyn}. According to the *Plaschke et al.* [2013] identification criterion (a jet region is where $P_{dyn}/P_{dyn}^{SW} > 0.25$ and has a peak >0.5), these high-pressure flows are magnetosheath jets. Summarizing, inside the magnetosheath we have regions of high-pressure flows, also called magnetosheath jets, and in one such flow is our selected current sheet.

Figure 1g shows the ion omnidirectional spectrogram. It clearly shows large variations throughout the interval. The regions of high-pressure flows are associated with ion spectra having distinct peaks around 500 eV to 1 keV, while in other intervals ions are more evenly spread across the energies. This indicates that in the regions of high-pressure flows ions are less thermalized and their properties are closer to the undisturbed solar wind.

2.2. Current Sheet Properties

Now we analyze the orientation and velocity of the current region. Minimum variance analysis on the magnetic field, downsampled to the electron velocities, and averaged over the four spacecraft for the time of the current sheet (00:24:22.0–00:24:22.4 UT) gives the local current sheet coordinate system: $L = [-0.30, -0.76, 0.58]$, $M = [0.42, 0.44, 0.79]$, and $N = [0.86, -0.48, -0.19]$ (GSE). The ratio of intermediate and minimum eigenvalues is about 60, suggesting that the current region is a planar current sheet. For this normal direction N we estimate the time delays at which the different spacecraft observe the current sheet and estimate the current sheet velocity, $V_{N,CS} \sim -150$ km s^{-1}, marked in Figure 4h. This velocity is comparable to but slightly slower than Vi_N (see Figure 4h). Thus, in the current sheet frame there is a net flow of plasma from the side of solar wind-like plasma to the side of the magnetosheath-like plasma. Combining the current sheet velocity with the duration of current sheet crossing, 0.4 s, gives an estimate of the current sheet thickness as $\sim$60km ($\sim 2.6\lambda_i$). Figures 2a and 2b show the position of the four spacecraft relative the current sheet in the N, L and N, M planes, respectively. Figure 2 shows the magnetic field in the LMN coordinate system for all four spacecraft, where Figure 2c shows the B_L component for all four spacecraft, while Figures 2d–2g show the magnetic field components in L, M, and N direction as well as the magnetic field magnitude time shifted to be aligned with the estimated current sheet location. We note that for a given time step the magnetic field can be quite different between the different spacecraft (see Figures 2d–2g). Because the spacecraft separation is slightly less than one ion inertial length, this indicates that sub-ion scale processes are at work in the current sheet, which could explain some of the observed differences. The magnetic field normal to the current sheet B_N is roughly constant across the current sheet for MMS1–MMS3, but MMS4 shows a significantly different value for almost 0.3 s within the current sheet. This indicates that the current sheet is not just a planar structure but shows internal structure on the scale of the spacecraft separation. The four spacecraft observe negative B_N values with an average of $B_N \sim -16$ nT. This suggests that the current sheet is not a tangential discontinuity, but instead that both sides of the current sheet are magnetically connected. We return to this point in section 3. In summary, four-spacecraft measurements have allowed us to estimate the current sheet's orientation, velocity, and thickness; and inside the current sheet we observe internal structuring at sub-ion kinetic scales.

Figure 3 gives a zoomed in view of the current sheet as seen by MMS4, except for one panel where multispacecraft data are used. Figure 3a shows the magnetic field. The current sheet interval is marked by the orange shaded area, and a jump in the magnetic field components can be clearly seen inside the current sheet. We also observe an increase in the magnitude of the magnetic field almost in the center of the current sheet (00:24:22.15 UT). Figure 3b shows the current estimated using the curlometer method [*Dunlop et al.*, 1988]. The highest current density, 4900 nA m^{-2}, is observed in the center of the current sheet. However, there is a significant current density in almost the entire interval starting from about 00:24:21UT. The current is mainly aligned with the local magnetic field in the antiparallel direction. One can also notice that both the magnetic field and the current show distinct fluctuations about 0.8s after the current sheet crossing. All this suggests that the current sheet is not a single well isolated structure that can be studied independent of the surrounding environment.

Figures 3c and 3d show the ion and electron velocities, respectively. The ion velocity shows that the values of V_Y and V_Z are closer to zero, while V_X shows an increase from about 200 km s^{-1} in the beginning of interval to about 250 km s^{-1} at the end of the interval. The electron velocity on a large scale is similar to the ion velocity; however, it shows much larger fluctuations correlated with the current. Thus, electrons are the dominant current carriers during the interval. The electron velocity peaks at the center of the current sheet.

Figure 3e shows the ion omnidirectional flux. It shows that right before the current sheet we have a warmer magnetosheath-like plasma, while right after the current sheet the ion spectrogram shows a narrower peak in energy corresponding to colder plasma and is thus more like the undisturbed solar wind but still warmer and denser than the pristine solar wind. The narrow peak in energy is clearest within the strong current region.

Figures 3f–3h show the electron distribution functions in the parallel, perpendicular, and antiparallel directions, respectively. The values for the colorbar have been selected so that the distribution function in the thermal range is well resolved. The high-energy edge of the thermal range is very sharp in the parallel direction, while for the antiparallel and perpendicular directions, it is relatively smooth. This suggests that the distributions in the antiparallel and perpendicular directions are more Maxwellian, while in the parallel direction the distributions show signs of parallel acceleration and corresponding flattop formation.

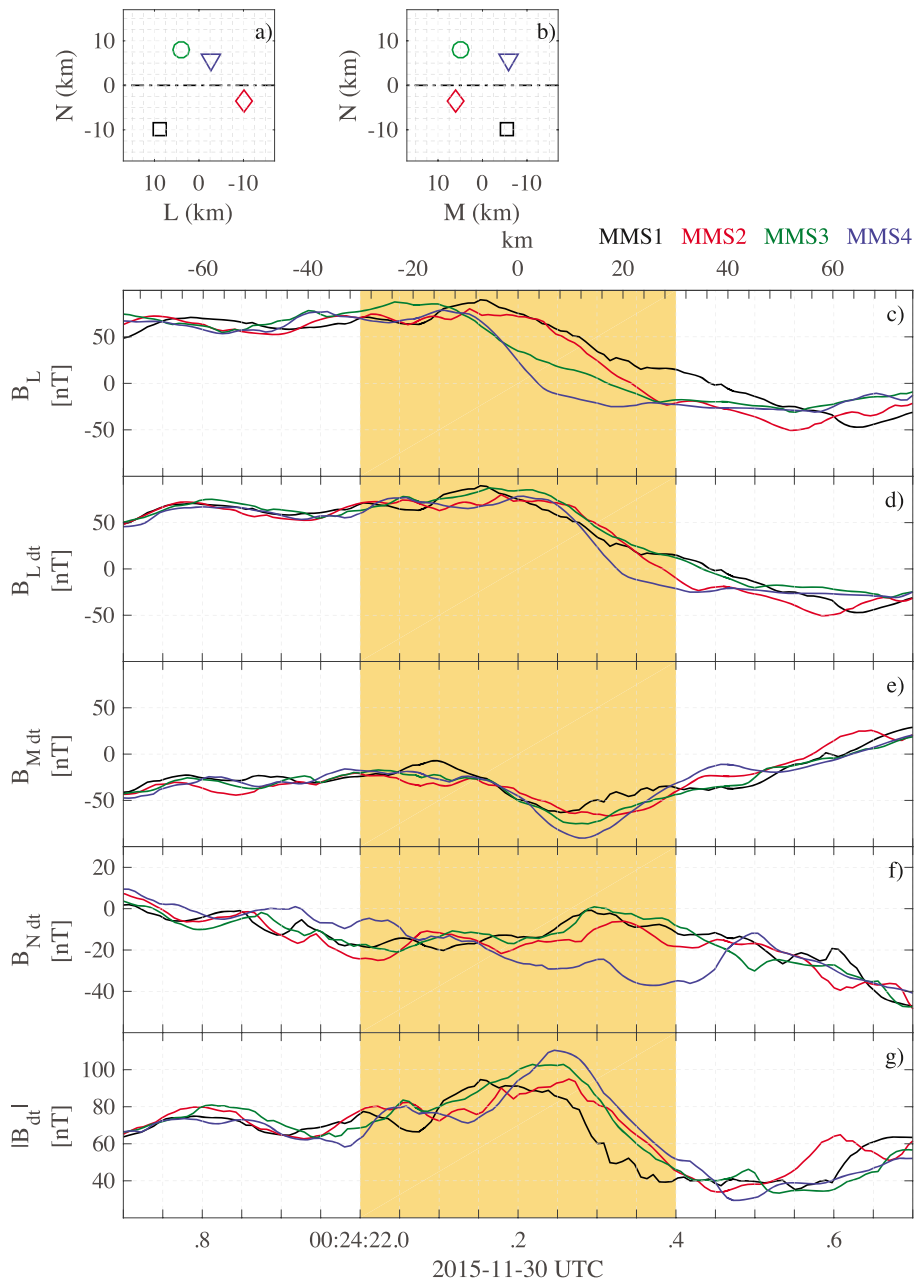

Figure 2. Spacecraft configuration and magnetic field from all spacecraft in *LMN* coordinates. (a and b) The position of the spacecraft in the *N*, *L* and *N*, *M* plane. The orientation of the current sheet is marked with a dash-dotted line, (c) the magnetic field from all four spacecraft in the *L* direction, (d–g) the magnetic field from all four spacecraft in the *L*, *M*, *N* direction, and absolute magnitude time shifted to the current sheet reference frame. The shaded orange area indicates the studied current sheet.

Detailed inspection of the parallel spectrogram shows that during some time intervals the distribution functions have peaks at higher energies that correspond to electron beams (Figure 5). Electron beams can be signs of ongoing local parallel acceleration, or they can be forming elsewhere and propagate into the region. The parallel distribution function spectrogram also clearly shows that the region just before and within the current sheet is where the parallel acceleration reaches the highest energies throughout the interval. Figure 3i shows the parallel and perpendicular electron temperatures. The region before and within the current sheet is associated with a temperature increase that is mostly in the parallel direction. In addition, the temperature of the region right after the current sheet (00:24:22.4 UT) is about 20 eV lower than the temperature of the region

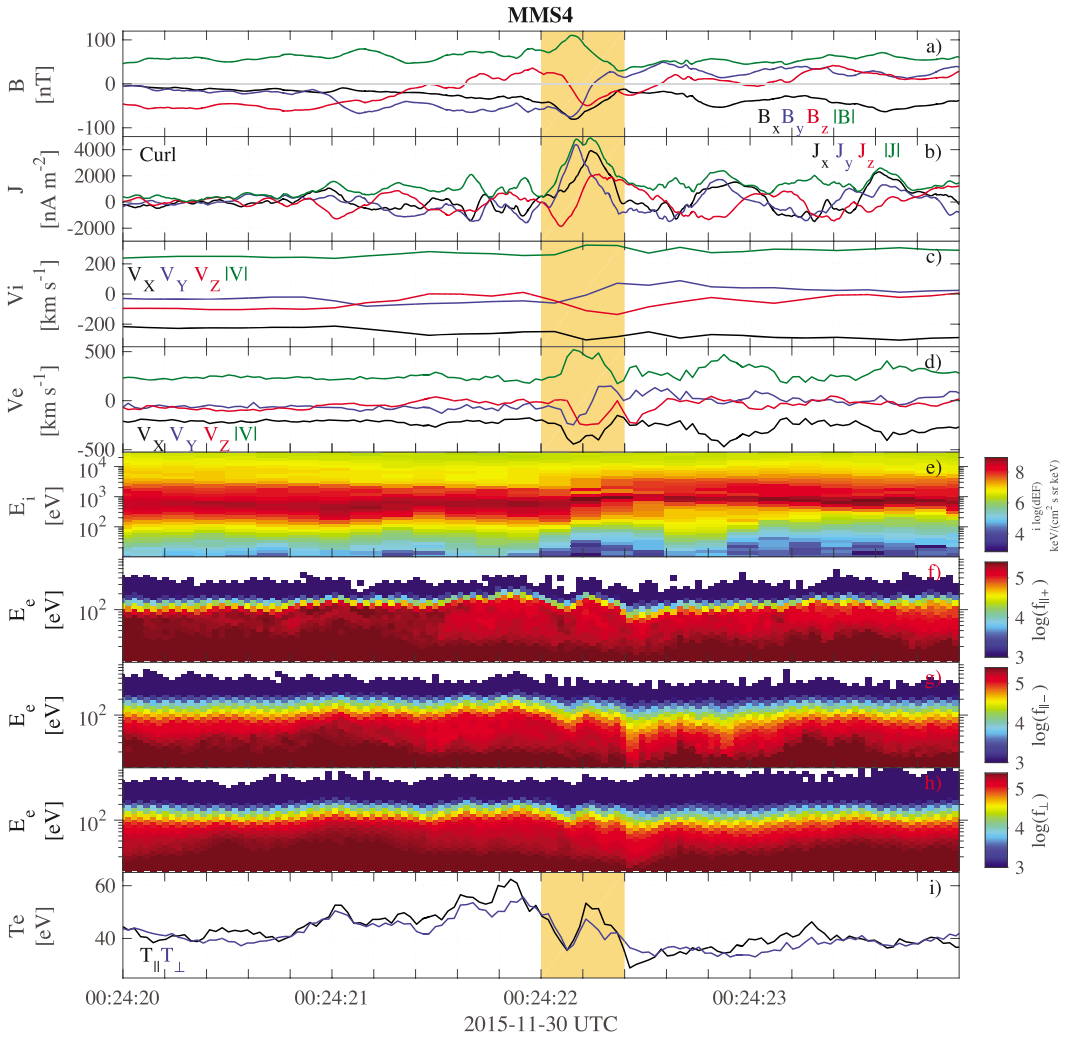

Figure 3. Overview of the current sheet. Unless otherwise stated, all coordinates are in GSE. (a) The magnetic field; (b) current; (c) ion velocity; (d) electron velocity; (e) ion omnidirectional fluxes; (f–h) parallel, antiparallel, and perpendicular electron distribution; and (i) parallel and perpendicular electron temperature. The orange shaded area indicates the studied current sheet.

right before the current sheet (00:24:21.8 UT). In summary, observations at the current sheet show signs of ongoing thermalization and parallel acceleration processes.

3. Discussion

The multispacecraft observations of the strong current region presented in Figure 2 suggest that it is not a simple planar current sheet. When the magnetic field is averaged over all spacecraft, the minimum variance result shows very good ratios between the *M*/*N* and *L*/*M* eigenvalues (61 and 6.1, respectively). This is a strong argument in favor of the current region being a current sheet on a larger scale. However, when the minimum variance method is applied to all magnetic field measurements from all four spacecraft (instead of averaging), the ratios of eigenvalues are significantly worse ($\lambda_M/\lambda_N = 5.5$, $\lambda_L/\lambda_M = 3.6$). This suggests that the current sheet shape is most likely not planar on the scale of the spacecraft separation. This is consistent with the large differences between spacecraft, tens of nanoteslas, seen in the magnetic field components plotted in the current sheet reference frame, see Figure 2. In addition, MMS4 observes a peak in magnetic field magnitude of almost 110nT, while, e.g., MMS1 does not have such a distinct peak and its value is less than 90nT. This shows that on a scale of the spacecraft separation there is a large difference in the magnetic field pressure. All this suggests that similar to the observations made by *Greco et al.* [2016] in the solar wind the strong current region has a complicated three-dimensional (3-D) structure on the scale of the spacecraft separation ($\sim \lambda_i$).

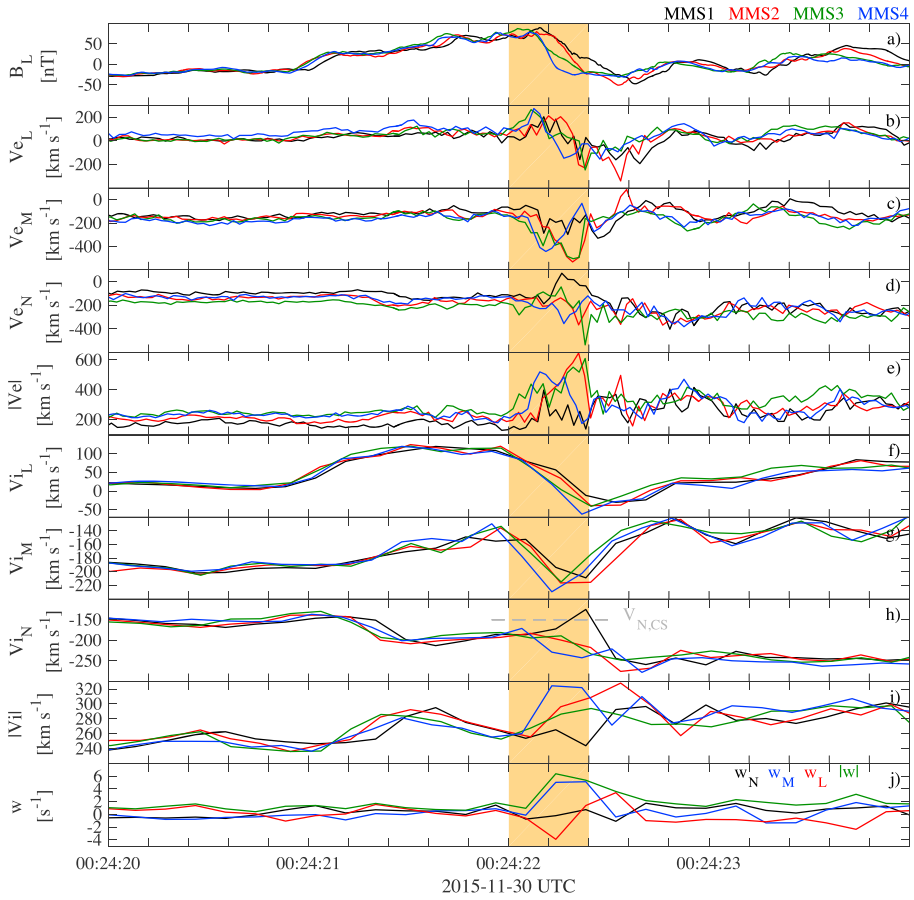

Figure 4. Multispacecraft observation of the current sheet in *LMN* coordinates. (a) The magnetic field in *L* direction; (b–d) the electron velocity in *L*, *M*, and *N* direction, respectively; (e) the magnitude of the electron velocity; (f–h) the ion velocity in *L*, *M*, and *N* direction, respectively, where the dotted grey line indicates the current sheet velocity along the normal; (i) the magnitude of the ion velocity; and (j) vorticity, *w*. The orange shaded area indicates the studied current sheet.

3.1. Current Sheet Formation

Next we discuss some possible formation mechanisms for such a strong current region. One possibility is that the current sheet is formed in the solar wind and crosses the bow shock into the magnetosheath. However, detailed analysis of magnetic field data from Themis B, Themis C, and Geotail (not shown), which were located in the solar wind when the current sheet was observed by MMS, shows no evidence of strong, thin current sheets. Therefore, the formation of the current sheet is most likely done locally. Figure 4 shows the magnetic field, the ion and electron velocities, and vorticity, $\mathbf{w} = \nabla \times \mathbf{V}_i$, in the *LMN* coordinate system for all four spacecraft. The strong current region, seen also as the large difference in B_L in Figure 4, is marked orange. On average, for both electrons and ions, V_M and V_N show larger velocities than V_L. However, the large-scale velocity variations in the region surrounding the current sheet are of the order 100 km s^{-1} in all components. This indicates that there is a velocity shear across the current sheet. Velocity shears are known to create thin, strong current sheet regions, possibly susceptible to instabilities, such as the Kelvin-Helmholtz instability. In addition, we observe large differences in velocities between the spacecraft both in ion and electron velocities. This indicates that significant velocity shears can be present on scales smaller than the spacecraft separation. This is also supported by a peak in the vorticity at the current sheet (Figure 4j). The difference in Vi_N between the beginning and end of the time interval is almost 100km s^{-1} with Vi_N being the largest at the end of the interval. There can be several explanations for such a jump in Vi_N. First, the current region can be forming at the front edge of a faster plasma jet (the end of the interval) penetrating a region with a smaller velocity (the beginning of the interval). Earlier studies have shown local shocks forming in regions of fast plasma jets

[*Hietala et al.*, 2009]. We can estimate the magnetosonic Mach number in the current sheet reference frame during the current sheet crossing

$$M_{MS} = \frac{|Vi_N - V_{N,CS}|}{V_{MS}}, \quad (1)$$

where V_{MS} is the fast magnetosonic wave speed along the current sheet normal. The M_{MS} values are all below 0.4 and thus the ion flow, in relation to the current sheet, is submagnetosonic. Thus, the current sheet is no local shock. Second, the difference in Vi_N could correspond to the inflows into a reconnecting current sheet. However, in this case the inflow speed would be about 50km s^{-1}, which is very large in comparison to the local Alfvén speed of about 100km s^{-1}. The relative reconnection rate of about 0.5 has not been reported earlier from simulations or observations, and thus this scenario does not seem probable. In summary, the thin current sheet is most likely formed locally due to velocity shear, but we cannot rule out other possibilities.

Observations show that the strong current region is located in a magnetosheath interval where the total pressure is over three times higher than the dynamic pressure in the undisturbed solar wind as estimated from OMNI data. During this interval the total pressure in the magnetosheath is dominated by dynamic pressure, similar to the undisturbed solar wind. The dominance of the dynamic pressure is an indicator for the presence of jets. Such magnetosheath jets downstream of a quasi-parallel shock have been found in both observational data and simulations before, and it has been suggested that they are created due to varying shock geometry [*Hietala et al.*, 2009, 2012; *Karimabadi et al.*, 2014; *Plaschke et al.*, 2016]. Because we expect such jets to form in localized regions, they will drive turbulence inside the magnetosheath and we expect velocity shears to form on the edges of those jets or in front of them as they interact with preexisting magnetosheath plasma. The velocity data in Figure 4 support the possibility of such a current sheet formation mechanism.

To study the current sheet in more detail, we performed the Walén test [*Khrabrov and Sonnerup*, 1998], using ion velocity and average magnetic field from all four spacecraft, on the interval surrounding the current sheet region, 00:24:21.7 UT–00:24:22.7 UT. The Walén test is acceptable with a slope of 0.66 and a correlation coefficient of 0.89. This supports the observation that both sides of the current sheet are magnetically connected, as is also seen by B_N being nonzero, and that there is a net plasma flow from one side of the current sheet to the other. A good Walén test is usually used to indicate reconnection, but there is no other clear reconnection signature observed; and therefore there is not sufficient evidence that reconnection is occurring within the current sheet. We cannot exclude the possibility that the internal structure within the current sheet is due to, for example, flux rope formation during reconnection, but this cannot explain the good Walén test using a larger time interval. It can even be that the current sheet starts reconnecting later as it propagates deeper into the magnetosheath since reconnecting current sheets inside the magnetosheath have been observed in earlier studies [*Retino et al.*, 2007; *Chasapis et al.*, 2015; *Yordanova et al.*, 2016].

3.2. Electron Beam Properties

Next we discuss the electron distributions around the current sheet. Observations suggest electron heating and parallel electron beam formation inside and near the current sheet region, Figures 3f–3i. The electron jet observed in the current sheet (Figure 3d) that carries the current is due to an electron beam (Figure 3f). The beam is in the direction parallel to the magnetic field, and to study the electron distribution function in more detail, we show the distribution function in the center of the current sheet in Figure 5. Figure 5a shows the 0°, 90°, and 180° pitch angle distributions versus energy. Figure 5b shows the full pitch angle distribution where the different colored lines indicate different energy levels. The electron beam can be seen in both panels between 80 and 200 eV and confined in the angular direction to pitch angles less than about 45°. The density and speed of the beam is about 15 cm^{-3} and 5.8 $\times 10^3$ km s^{-1}, respectively, which is almost 10% of the total electron density with an electron beam energy (~100 eV) of about twice the electron thermal energy. At higher energies of about 210–450 eV, which are above the beam energy, there is a decrease in the electron distribution in the parallel direction. Thus, something similar to a loss cone is formed at those energies and suggests that there are high-energy magnetosheath-like electrons heading toward the solar wind-like plasma and escaping. The loss cone size in this scenario is determined by the ratio of local magnetic field magnitude and the peak magnetic field magnitude along the electron path into the solar wind-like plasma. In such a case we expect to observe loss cone pitch angles close to 90° when the spacecraft observes the largest magnetic field magnitude. The observations are consistent with this; Figure 3a shows that MMS4 observes the largest magnetic field magnitude at about 00:24:22.12 UT, and around this time the loss cone angle is close to 90°.

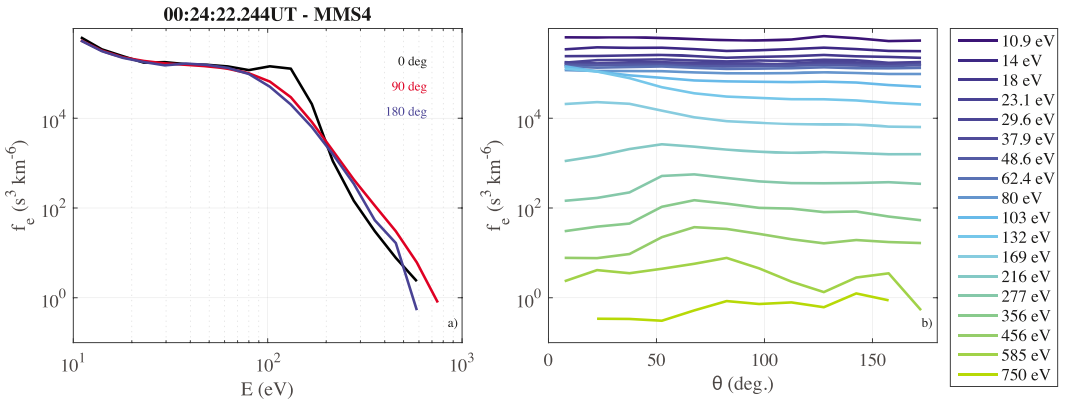

Figure 5. Detailed plots of the electron distribution function. (a) Electron distribution in parallel, antiparallel, and perpendicular pitch angle direction. (b) The full electron pitch angle distribution where the different energies are given by the color of the lines.

Thus, around that time all observed high-energy magnetosheath-like electrons escape into the solar wind-like plasma. In summary, at energies comparable to and below the beam energy solar wind-like electrons are accelerated and penetrate the magnetosheath-like plasma, and at higher energies we observe a loss cone due to magnetosheath-like electrons escaping into the solar wind-like plasma.

The electron beams inside the current sheet are most likely formed locally in the magnetosheath due to acceleration from an electrostatic potential difference along the ambient magnetic field. Electron beams are observed continuously in the interval, see Figure 3f. When analyzing Figures 3f–3h in more detail, we see that the beams are always in the parallel direction, indicating a parallel acceleration mechanism. However, despite the continuous observation of beams along the whole interval (Figure 3f), there are observations suggesting that the beam generation is ongoing throughout the current sheet, as the properties of the electron population shift from a cold solar wind-like to a hot thermalized magnetosheath-like population. There are two main observations suggesting that the electron beams inside the current sheet are locally generated. First, local acceleration requires a local parallel electric field. The strong field-aligned current in the current sheet, where we observe electron beams with the highest energy, suggests the possibility of formation of such a parallel electric field. Second, the beams observed in the end and beginning of the interval (Figure 3f) are more diffused than the ones observed right before and inside the current sheet. More diffused beams have lower beam energies, and their slope in the parallel distribution function, at energies above the peak beam energy, is flatter. This could be due to wave-particle interactions which with time will diffuse an electron beam making its slope at higher energies flatter with a lower peak beam energy and contribute to the heating of the plasma. Thus, more diffuse electron beams have formed farther away. This is consistent with observations of different electrostatic waves in the regions of strong current (not shown), which are most likely generated by the locally accelerated electron beams. All these observations fit well with the theory of electron acceleration proposed by *Feldman et al.* [1983] commonly used to explain electron acceleration across a shock due to a change in electrostatic potential. However, in our case, the electron acceleration is occurring inside the magnetosheath. Thus, our observations indicate that electron acceleration due to electrostatic potential jumps also occurs locally inside the magnetosheath and not just across the bow shock. Therefore, electron beams observed in the magnetosheath do not have to originate from the bow shock.

4. Conclusions

We present detailed kinetic observations of a strong, narrow current sheet at a fast magnetosheath jet downstream of a quasi-parallel shock. The current sheet has a thickness of about 3 λ_i and is propagating approximately antisunward with a speed of ~150 km s^{-1}. Different minimum variance analysis results from average, and all multispacecraft magnetic field measurements indicate that the current sheet is not a simple planar structure but has a complex 3-D geometry. The current sheet is observed within a magnetosheath jet with dynamic pressure significantly higher than the solar wind dynamic pressure. The jet is submagnetosonic in relation to the current sheet. The current sheet is formed at the boundary between a colder, more solar wind-like, plasma and warmer, magnetosheath-like, plasma. Large velocity shears are present in the

region of the current sheet and can be the cause of its formation. The velocity shears themselves are most likely due to the magnetosheath jet. The current sheet has a strong 16 nT normal component of the magnetic field, and there is a net plasma flow across the current sheet, which is consistent with our Walén test result. However, there are not enough signatures to confirm that reconnection is occurring within the current sheet. We speculate that this current sheet may reconnect as it propagates deeper into the magnetosheath.

Inside the current sheet we observe electron acceleration parallel to the magnetic field corresponding to acceleration toward Earth. Almost 10% of the electron density, corresponding to 15 cm^{-3}, is in the beam, and the energy of electrons in the beam is ~100 eV, corresponding to about twice the electron thermal energy. The electron beam may be responsible for part of the electron heating due to wave-particle interactions in the magnetosheath plasma. Our observations at the current sheet suggest that the electron beams are forming locally due to a difference in the electrostatic potential along the ambient magnetic field. In addition, we observe a loss cone at energies above the beam energy, which is consistent with hot magnetosheath-like electrons escaping sunward. Similar features of electron beams and loss cones have been observed at the bow shock due to acceleration from a change in the electrostatic potential across the shock [*Feldman et al.*, 1983]. Here we show evidence that such an acceleration process can work not only at the shock but also at current sheets farther inside the magnetosheath.

Acknowledgments
We thank the entire MMS team and instrument PIs for data access and support. We also thank the OMNI data for giving us access to the solar wind data used in this study. We acknowledge NASA contract NAS5-02099 and V. Angelopoulos for the use of data from the THEMIS mission. Specifically, K.H. Glassmeier, U. Auster, and W. Baumjohann for the use of FGM data provided under the lead of the Technical University of Braunschweig and with financial support through the German Ministry for Economy and Technology and the German Center for Aviation and Space (DLR) under contract 50 OC 0302. We thank S. Kokubun for the use of GEOTAIL MGF data. The authors acknowledge the support by the International Space Science Institute (ISSI) in Bern, Switzerland, and the ISSI team *Particle Acceleration in Solar Flares and Terrestrial Substorms*. We also thank T. Karlsson, W. Li, and A. Johlander for useful discussions. This work was supported by the Swedish Research Council, grant 2013-4309. MMS data are available at https://lasp.colorado.edu/mms/sdc/public. Themis, OMNI, and Geotail data are available at http://cdaweb.gsfc.nasa.gov/istp_public/.

References

Archer, M. O., and T. S. Horbury (2013), Magnetosheath dynamic pressure enhancements: Occurrence and typical properties, *Ann. Geophys.*, *31*(2), 319–331, doi:10.5194/angeo-31-319-2013.

Birn, J., and E. R. Priest (2007), *Reconnection of magnetic fields*, Cambridge Univ. Press, Cambridge, U. K., doi:10.1017/CBO9780511536151.

Burch, J. L., T. E. Moore, R. B. Torbert, and B. L. Giles (2016), Magnetospheric multiscale overview and science objectives, *Space Sci. Rev.*, *199*(1), 5–21, doi:10.1007/s11214-015-0164-9.

Chasapis, A., A. Retinò, F. Sahraoui, A. Vaivads, Y. V. Khotyaintsev, D. Sundkvist, A. Greco, L. Sorriso-Valvo, and P. Canu (2015), Thin current sheets and associated electron heating in turbulent space plasma, *Astrophys. J.*, *804*(1), L1, doi:10.1088/2041-8205/804/1/L1.

Dunlop, M. W., D. J. Southwood, K. H. Glassmeier, and F. M. Neubauer (1988), Analysis of multipoint magnetometer data, *Adv. Space Res.*, *8*(9-10), 273–277, doi:10.1016/0273-1177(88)90141-X.

Ergun, R. E., et al. (2016), The axial double probe and fields signal processing for the MMS mission, *Space Sci. Rev.*, *199*, 167–188, doi:10.1007/s11214-014-0115-x.

Farris, M. H., and C. T. Russell (1994), Determining the standoff distance of the bow shock: Mach number dependence and use of models, *J. Geophys. Res.*, *99*, 681–689.

Feldman, W. C., R. C. Anderson, S. J. Bame, S. P. Gary, J. T. Gosling, D. J. Mccomas, M. F. Thomsen, G. Paschmann, and M. M. Hoppe (1983), Electron velocity distributions near the Earth's bow shock, *J. Geophys. Res.*, *88*(A1), 96–110, doi:10.1029/JA088iA01p00096.

Greco, A., P. Chuychai, W. H. Matthaeus, S. Servidio, and P. Dmitruk (2008), Intermittent MHD structures and classical discontinuities, *Geophys. Res. Lett.*, *35*, L19111, doi:10.1029/2008GL035454.

Greco, A., S. Perri, S. Servidio, E. Yordanova, and P. Veltri (2016), The complex structure of magnetic field discontinuities in the turbulent solar wind, *Astrophys. J. Lett.*, *823*(2), L39.

Hao, Y., B. Lembege, Q. Lu, and F. Guo (2016), Formation of downstream high-speed jets by a rippled nonstationary quasi-parallel shock: 2-D hybrid simulations, *J. Geophys. Res. Space Physics*, *121*, 2080–2094, doi:10.1002/2015JA021419.

Hietala, H., et al. (2009), Supermagnetosonic jets behind a collisionless quasiparallel shock, *Physical Rev. Lett.*, *103*(24), 20–23, doi:10.1103/PhysRevLett.103.245001.

Hietala, H., et al. (2012), Supermagnetosonic subsolar magnetosheath jets and their effects: From the solar wind to the ionospheric convection, *Ann. Geophys.*, *30*(1), 33–48, doi:10.5194/angeo-30-33-2012.

Karimabadi, H., et al. (2014), The link between shocks, turbulence, and magnetic reconnection in collisionless plasmas, *Phys. Plasmas*, *21*, 62308, doi:10.1063/1.4882875.

Khrabrov, A. V., and B. U. Ö. Sonnerup (1998), DeHoffmann-Teller analysis, *ISSI Sci. Rep. Ser.*, *1*, 221–248.

King, J. H., and N. E. Papitashvili (2005), Solar wind spatial scales in and comparisons of hourly Wind and ACE plasma and magnetic field data, *J. Geophys. Res.*, *110*, A02104, doi:10.1029/2004JA010649.

Lindqvist, P.-A., et al. (2016), The spin-plane double probe electric field instrument for MMS, *Space Sci. Rev.*, *199*, 137–165, doi:10.1007/s11214-014-0116-9.

Mikhailovskii, A. (1974), *Instabilities of an Inhomogeneous Plasma*, vol. 2, Springer, New York.

Omidi, N., J. Berchem, D. Sibeck, and H. Zhang (2016), Impacts of spontaneous hot flow anomalies on the magnetosheath and magnetopause, *J. Geophys. Res. Space Physics*, *121*, 3155–3169, doi:10.1002/2015JA022170.

Plaschke, F., H. Hietala, and V. Angelopoulos (2013), Anti-sunward high-speed jets in the subsolar magnetosheath, *Ann. Geophys.*, *31*(10), 1877–1889, doi:10.5194/angeo-31-1877-2013.

Plaschke, F., H. Hietala, V. Angelopoulos, and R. Nakamura (2016), Geoeffective jets impacting the magnetopause are very common, *J. Geophys. Res. Space Physics*, *121*, 3240–3253, doi:10.1002/2016JA022534.

Pollock, C., et al. (2016), Fast plasma investigation for magnetospheric multiscale, *Space Sci. Rev.*, *199*, 331–406, doi:10.1007/s11214-016-0245-4.

Priest, E. R., and T. G. Forbes (2000), *Magnetic reconnection: MHD theory and applications*, 596 pp., Cambridge Univ. Press, New York, doi:10.1029/EO065i013p00124.

Retino, A., D. Sundkvist, A. Vaivads, F. Mozer, M. Andre, and C. Owen (2007), In situ evidence of magnetic reconnection in turbulent plasma, *Nat. Phys.*, *3*(4), 236–238, doi:10.1038/nphys574.

Russell, C. T., et al. (2016), The Magnetospheric multiscale magnetometers, *Space Sci. Rev.*, *199*, 189–256, doi:10.1007/s11214-014-0057-3.

Servidio, S., W. H. Matthaeus, M. A. Shay, P. A. Cassak, and P. Dmitruk (2009), Magnetic reconnection in two-dimensional magnetohydrodynamic turbulence, *Phys. Rev. Lett.*, *102*(11), 115003, doi:10.1103/PhysRevLett.102.115003.

Servidio, S., F. Valentini, D. Perrone, A. Greco, F. Califano, W. H. Matthaeus, and P. Veltri (2015), A kinetic model of plasma turbulence, *J. Plasma Phys.*, *81*(1), 10107, doi:10.1017/S0022377814000841.

Shue, J.-H., et al. (1998), Magnetopause location under extreme solar wind conditions, *J. Geophys. Res.*, *103*(A8), 17,691–17,700, doi:10.1029/98JA01103.

Vörös, Z., E. Yordanova, M. M. Echim, G. Consolini, and Y. Narita (2016), Turbulence-generated proton-scale structures in the terrestrial magnetosheath, *Astrophys. J.*, *819*(1), L15, doi:10.3847/2041-8205/819/1/L15.

Wan, M., W. Matthaeus, V. Roytershteyn, H. Karimabadi, T. Parashar, P. Wu, and M. Shay (2015), Intermittent dissipation and heating in 3D kinetic plasma turbulence, *Phys. Rev. Lett.*, *114*(17), 175002, doi:10.1103/PhysRevLett.114.175002.

Yordanova, E., et al. (2016), Electron scale structures and magnetic reconnection signatures in the turbulent magnetosheath, *Geophys. Res. Lett.*, *43*, 5969–5978, doi:10.1002/2016GL069191.